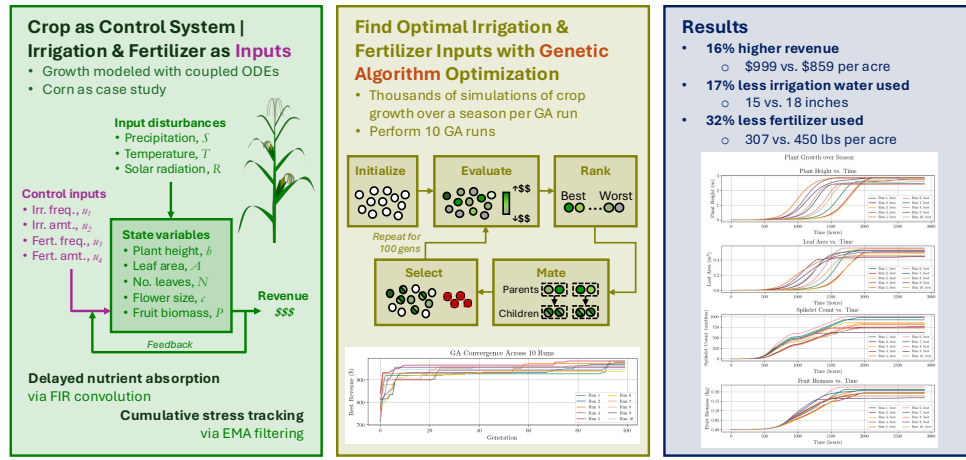


1 Graphical Abstract

2 Optimizing irrigation and fertilizer strategy using a crop growth model with delayed nutrient absorption dynamics

4 Carla J. Becker, Tarek I. Zohdi

Optimizing Irrigation & Fertilizer Strategy via Crop Model + Genetic Algorithm



UC Berkeley Carla J. Becker, Tarek I. Zohdi (2026)

5 Highlights

6 **Optimizing irrigation and fertilizer strategy using a crop growth**
7 **model with delayed nutrient absorption dynamics**

8 Carla J. Becker, Tarek I. Zohdi

- 9 • Reduced-order coupled ODE model; efficient alternative to DSSAT/AP-
10 SIM
- 11 • FIR convolution formulation for delayed nutrient absorption dynamics
- 12 • EMA filtering for cumulative environmental stress tracking
- 13 • GA optimization of irrigation/fertilization schedules to maximize rev-
14 enue
- 15 • Calibration and validation against Iowa corn agronomic data

16 Optimizing irrigation and fertilizer strategy using a crop
17 growth model with delayed nutrient absorption
18 dynamics

19 Carla J. Becker, Tarek I. Zohdi

^a*Department of Mechanical Engineering, University of California, Berkeley, 6141
Etcheverry Hall, Berkeley, 94720, California, United States of America*

^b*Department of Mechanical Engineering, University of California, Berkeley, 6141
Etcheverry Hall, Berkeley, 94720, California, United States of America*

20 **Abstract**

21 **CONTEXT** Rising production costs and declining commodity prices have
22 motivated farmers to seek computational tools for optimizing resource appli-
23 cation. While sophisticated crop models such as DSSAT and APSIM simulate
24 detailed physiological processes, they require extensive parameterization and
25 may be computationally expensive for optimization applications. Moreover,
26 existing optimization approaches often use simplified plant response models
27 that do not capture the delayed, cumulative effects of resource application.

28
29 **OBJECTIVE** This study develops a reduced-order crop growth model that
30 captures delayed nutrient absorption dynamics and couples it with a genetic
31 algorithm to optimize irrigation and fertilizer strategies that maximize net
32 revenue while minimizing input costs.

33
34 **METHODS** We present a generalized, coupled ordinary differential equa-
35 tion (ODE) model tracking five state variables—plant height, leaf area, num-
36 ber of leaves, flower size, and fruit biomass—each governed by logistic growth
37 with time-varying growth rates and carrying capacities. These parameters
38 are modulated by nutrient factors quantifying how well actual water, fertil-
39 izer, temperature, and solar radiation levels match expected values. Delayed
40 physiological response is captured using finite impulse response (FIR) con-
41 volution with Gaussian kernels, where different temporal spreads represent
42 distinct metabolic timescales for each input type. Cumulative stress from sus-
43 tained deviations is tracked using exponential moving average (EMA) filters.

⁴⁴ A genetic algorithm searches over application frequency and amount for both
⁴⁵ irrigation and fertilizer, evaluating candidate strategies through full-season
⁴⁶ simulations. The framework is demonstrated using corn grown in Fairfax,
⁴⁷ Iowa, with historical weather data under a drought scenario (50% of typical
⁴⁸ precipitation).

⁴⁹

⁵⁰ **RESULTS AND CONCLUSIONS** The genetic algorithm identifies non-
⁵¹ intuitive strategies that outperform conventional uniform application sched-
⁵² ules, achieving 16% higher net revenue (\$999 vs. \$859 per acre) through
⁵³ strategic timing of resource inputs. The optimized strategies use 17% less ir-
⁵⁴ rigation (15 vs. 18 inches) and 32% less fertilizer (307 vs. 450 lbs) than farmer
⁵⁵ best practices while achieving comparable or higher crop yields. Across 10
⁵⁶ independent optimization runs, 9 outperformed the baseline, demonstrating
⁵⁷ algorithm robustness.

⁵⁸

SIGNIFICANCE These results demonstrate that under delayed absorption dynamics, timing of inputs matters more than total quantity—a finding that challenges conventional drought response strategies of increased irrigation frequency. The framework offers a computationally tractable alternative to complex mechanistic models for precision agriculture optimization and is generalizable to other crops through re-parameterization.

⁵⁹ *Keywords:* precision agriculture, resource optimization, crop growth
⁶⁰ model, genetic algorithm, cumulative stress tracking

⁶¹ **1. Introduction**

⁶² The agriculture sector in the United States faces significant challenges as
⁶³ the number of farms declines and the cost of farming continues to rise [1].
⁶⁴ Rising production expenses for equipment, seeds, and labor, coupled with
⁶⁵ elevated interest rates and declining commodity prices, have made farming
⁶⁶ increasingly expensive. To navigate this challenging landscape, farmers are
⁶⁷ employing strategies such as cost management and operational optimiza-
⁶⁸ tion. One promising approach is to use modeling and simulation to optimize
⁶⁹ farm operations without substantial capital investment. Recent advances in
⁷⁰ computational methods have enabled sophisticated digital-twin frameworks
⁷¹ for precision agriculture [2, 3], and machine learning techniques have been

72 applied to optimize sensor placement and resource delivery in agricultural
73 systems [4, 5].

74 Mathematical modeling of crop growth has a rich history, with models
75 ranging from simple empirical relationships to complex mechanistic simulations.
76 Logistic growth models, first proposed by Verhulst in 1838, remain
77 widely used due to their interpretability and ability to capture resource-
78 limited growth dynamics [6]. More sophisticated crop models such as DSSAT
79 [7], APSIM [8], and WOFOST [9] simulate detailed physiological processes
80 but require extensive parameterization and may be computationally expen-
81 sive for optimization applications. In contrast, reduced-order models that
82 capture essential dynamics while remaining tractable for optimization have
83 gained attention in precision agriculture [10].

84 Optimization of irrigation and fertilizer application has been studied us-
85 ing various approaches, including linear and nonlinear programming [11],
86 dynamic programming [12], and metaheuristic algorithms [13]. Genetic algo-
87 rithms (GAs) are particularly well-suited for this domain because they can
88 handle nonlinear, non-convex objective functions and do not require gradi-
89 ent information [14]. Previous work has applied GAs to irrigation scheduling
90 [15] and fertilizer optimization [16], but these studies often use simplified
91 plant response models that do not capture the delayed, cumulative effects of
92 resource application.

93 This paper presents a generalized, coupled ordinary differential equation
94 (ODE) model for crop growth that addresses these limitations. The model
95 captures: (1) nonlinear logistic growth with state-dependent carrying ca-
96 pacities, (2) delayed absorption of water, fertilizer, temperature, and solar
97 radiation inputs through finite impulse response (FIR) convolution, (3) cu-
98 mulative stress tracking via exponential moving average (EMA) filters, and
99 (4) coupling between vegetative and reproductive growth stages. The model
100 is designed to enable global optimization under delayed, resource-coupled
101 dynamics—a regime where even well-established management practices may
102 benefit from computational refinement due to the sheer number of possible
103 scheduling combinations.

104 We demonstrate the framework by optimizing irrigation and fertilizer
105 strategies for corn, the most widely planted crop in the United States by
106 acreage. Using a genetic algorithm, we search for strategies that maximize
107 net revenue (crop value minus input costs) over a growing season. The ap-
108 proach is validated using historical weather data from Fairfax, Iowa, a rep-
109 resentative location in the Corn Belt.

110 **2. Generalized, coupled-ODE crop model**

111 The proposed model tracks five state variables representing key aspects
 112 of plant development: plant height h (m), leaf area per leaf A (m^2), num-
 113 ber of leaves N , flower size c (number of spikelets), and fruit biomass P
 114 (kg). Each state variable follows logistic growth dynamics with time-varying
 115 growth rates and carrying capacities that depend on environmental condi-
 116 tions and resource availability.

117 The model receives four input signals: water from irrigation w (inches),
 118 fertilizer application f (lbs), ambient temperature T ($^\circ\text{C}$), and solar radiation
 119 R (W/m^2). Precipitation S (inches) is added to irrigation to obtain total
 120 water input. Temperature and radiation data are obtained from the National
 121 Solar Radiation Database (NSRDB) [17], while precipitation data comes from
 122 NOAA historical records [18].

123 *2.1. Delayed absorption via FIR convolution*

124 Plants do not immediately process applied nutrients; instead, there is
 125 a physiologically-mediated delay between application and utilization. We
 126 model this delayed absorption using finite impulse response (FIR) convolu-
 127 tion with Gaussian kernels.

128 If cumulative nutrient uptake follows a sigmoid trajectory—with slow ini-
 129 tial uptake due to transport lag, rapid increase once metabolic pathways acti-
 130 vate, and eventual saturation—then instantaneous absorption rate follows a
 131 bell-shaped curve. A Gaussian kernel is the least assumptive choice for a bell
 132 curve, requiring only two parameters: the temporal spread σ (characterizing
 133 absorption duration) and the peak delay μ .

134 Given only the temporal spread σ for each nutrient type, we determine μ
 135 such that 95% of the kernel mass lies within $[0, 2\mu]$. This requires solving

$$\operatorname{erf}\left(\frac{\mu}{\sigma\sqrt{2}}\right) = 0.95, \quad (1)$$

136 which yields $\mu \approx 1.96\sigma$. The Gaussian FIR kernel is then

$$g[k] = \frac{1}{\sqrt{2\pi\sigma^2}} \exp\left\{-\frac{1}{2}\frac{(k-\mu)^2}{\sigma^2}\right\}. \quad (2)$$

137 The FIR horizon L^* is chosen as the minimum length capturing 95% of
 138 the kernel mass:

$$L^* = \min_L \left\{ L : \frac{\sum_{k=0}^{L-1} g[k]}{\sum_{k=0}^{K-1} g[k]} \geq 0.95 \right\} \quad (3)$$

139 where K is the simulation length in hours.

140 Different nutrients have different metabolic timescales. We use $\sigma_w = 30$
141 hours for water (rapid uptake), $\sigma_f = 300$ hours for fertilizer (slow uptake re-
142 flecting root absorption dynamics), and $\sigma_T = \sigma_R = 30$ hours for temperature
143 and radiation (immediate physiological effects with short memory).

144 *2.2. Cumulative stress tracking via EMA filtering*

145 While FIR convolution captures delayed absorption, plants also accumu-
146 late stress from sustained deviations from optimal conditions. We model this
147 cumulative effect using exponential moving average (EMA) filters, which are
148 equivalent to first-order infinite impulse response (IIR) systems.

149 The EMA filter with memory parameter $\beta \in [0, 1)$ has the recursive form:

$$y[k] = (1 - \beta)x[k] + \beta y[k - 1] \quad (4)$$

150 where larger β values correspond to longer memory (slower response to
151 changes). This formulation preserves constant signals ($x[k] = c$ implies
152 $y[k] \rightarrow c$) while smoothing transient fluctuations.

153 *2.3. Nutrient factor calculation*

154 We now describe the complete transformation pipeline that converts raw
155 input signals into nutrient factors $\nu \in [0, 1]$ that modulate plant growth. Us-
156 ing fertilizer as an example (the same process applies to water, temperature,
157 and radiation):

158 **Step 1: Delayed absorption.** Convolve the raw fertilizer signal $f[k]$
159 with the Gaussian FIR kernel:

$$\bar{f}[k] = \sum_{n=0}^{L_f-1} g_f[n] f[k - n] \quad (5)$$

160 **Step 2: Cumulative absorption.** Compute the running sum of ab-
161 sorbed fertilizer:

$$F[k] = \sum_{n=0}^k \bar{f}[n] \quad (6)$$

162 **Step 3: Instantaneous anomaly.** Compare actual cumulative absorp-
163 tion to expected levels:

$$\delta_f[k] = \left| \frac{k \cdot f_{\text{typ}} - F[k]}{k \cdot f_{\text{typ}} + \epsilon} \right| \quad (7)$$

164 where f_{typ} is the typical hourly fertilizer level the plant “expects” and ϵ is a
165 small constant preventing division by zero.

166 **Step 4: Cumulative divergence.** Apply EMA smoothing to track
167 sustained anomalies:

$$\Delta_f[k] = \beta_\Delta \Delta_f[k - 1] + (1 - \beta_\Delta) \delta_f[k] \quad (8)$$

168 where $\beta_\Delta = 0.95$ provides long memory.

169 **Step 5: Nutrient factor.** Convert divergence to a stress factor via
170 exponential decay with additional EMA smoothing:

$$\nu_f[k] = \beta_\nu \nu_f[k - 1] + (1 - \beta_\nu) \exp\{-\alpha \Delta_f[k]\} \quad (9)$$

171 where $\alpha = 3$ ensures $\nu \approx 0.05$ when $\Delta = 1$ (complete divergence from
172 expected levels), and $\beta_\nu = 0.05$.

173 The nutrient factor $\nu_f[k]$ equals 1 when fertilizer application perfectly
174 matches expected levels and decays toward 0 under sustained over- or under-
175 application. This captures the intuition that plants are resilient to brief
176 deviations but suffer cumulative damage from prolonged stress.

177 Figure 1 illustrates the FIR convolution and EMA smoothing operations
178 that constitute the metabolic transformation pipeline. The left panel shows
179 how the Gaussian FIR kernel spreads and delays input signals, while the
180 right panel demonstrates how EMA filtering with different β values tracks
181 cumulative divergence with varying memory lengths.

182 2.4. Effects of inputs on plant growth

183 Different inputs affect different aspects of plant growth. Tables 1 and 2
 184 summarize these relationships based on agronomic literature [19, 20, 21].

State variable	Irrigation on growth rate	Fertilizer on growth rate	Irrigation on capacity	Fertilizer on capacity
Plant height h	~	+	~	+
Leaf area A	~	+	+	+
Number of leaves N	~	~	~	~
Flower size c	~	~	+	~
Fruit biomass P	~	~	+	+

Table 1: Effects of irrigation and fertilizer on growth dynamics. “+” indicates positive effect, “~” indicates a negligible effect.

State variable	Temp. on growth rate	Temp. on capacity	Radiation on growth rate	Radiation on capacity
Plant height h	+	+	+	+
Leaf area A	+	+	+	+
Number of leaves N	~	+	~	+
Flower size c	-	-	-	-
Fruit biomass P	+	+	+	+

Table 2: Effects of temperature and solar radiation on growth dynamics. “+” indicates positive effect, “~” indicates a negligible effect, “-” indicates a negative effect. For flower size, excess heat and radiation reduce flower development, hence negative effects.

185 2.5. Growth dynamics

186 Each state variable follows logistic growth with time-varying parameters
 187 modulated by nutrient factors. The general form is:

$$\frac{dx}{dt} = \hat{a}_x(t) \cdot x(t) \left(1 - \frac{x(t)}{\hat{k}_x(t)} \right) \quad (10)$$

188 where $\hat{a}_x(t)$ is the effective growth rate and $\hat{k}_x(t)$ is the effective carrying
 189 capacity, both functions of the nutrient factors.

190 The effective parameters are computed as geometric means of the relevant
 191 nutrient factors, reflecting multiplicative rather than additive effects. This
 192 choice is motivated by the observation that growth rates compound over
 193 time, making geometric averaging appropriate [22].

194 **Plant height** responds to fertilizer, temperature, and radiation:

$$\hat{a}_h(t) = a_h(\nu_f \nu_T \nu_R)^{1/3}, \quad \hat{k}_h(t) = k_h(\nu_f \nu_T \nu_R)^{1/3} \quad (11)$$

195 **Leaf area** additionally depends on water and is coupled to height:

$$\hat{a}_A(t) = a_A(\nu_f \nu_T \nu_R)^{1/3}, \quad \hat{k}_A(t) = k_A \left(\nu_w \nu_f \nu_T \nu_R \frac{\hat{k}_h}{k_h} \right)^{1/5} \quad (12)$$

196 **Number of leaves** depends only on temperature and radiation through
 197 the carrying capacity:

$$\hat{a}_N(t) = a_N, \quad \hat{k}_N(t) = k_N(\nu_T \nu_R)^{1/2} \quad (13)$$

198 **Flower size** (spikelet count) exhibits inverse dependence on temperature
 199 and radiation—excess heat and light reduce flowering:

$$\hat{a}_c(t) = a_c \left(\frac{1}{\nu_T} \frac{1}{\nu_R} \right)^{1/2}, \quad \hat{k}_c(t) = k_c \left(\nu_w \frac{1}{\nu_T} \frac{1}{\nu_R} \right)^{1/3} \quad (14)$$

200 **Fruit biomass** depends on all inputs and is coupled to vegetative growth:

$$\hat{a}_P(t) = a_P \left(\frac{1}{\nu_T} \frac{1}{\nu_R} \right)^{1/2}, \quad \hat{k}_P(t) = k_P \left(\nu_w \nu_f \nu_T \nu_R \frac{\hat{k}_h \hat{k}_A \hat{k}_c}{k_h k_A k_c} \right)^{1/7} \quad (15)$$

201 The coupling terms \hat{k}_h/k_h , \hat{k}_A/k_A , and \hat{k}_c/k_c encode physiological depen-
 202 dencies: taller plants with more leaf area can support larger fruit, while larger
 203 tassels (more spikelets) may compete with ear development.

204 2.6. Model parameters

205 The baseline growth rates and carrying capacities are crop-specific pa-
 206 rameters that can be estimated from field data or literature values. For corn,
 207 we use the values in Table 3, calibrated to match typical development time-
 208 lines where plants reach full vegetative size around 65–70 days after sowing
 209 and grain fill completes around 125 days [23].

State	Growth rate	Carrying capacity	Initial condition	Units
Height h	$a_h = 0.010 \text{ hr}^{-1}$	$k_h = 3.0$	$h_0 = 0.001$	m
Leaf area A	$a_A = 0.0105 \text{ hr}^{-1}$	$k_A = 0.65$	$A_0 = 0.001$	m^2
Leaves N	$a_N = 0.011 \text{ hr}^{-1}$	$k_N = 20$	$N_0 = 0.001$	count
Spikelets c	$a_c = 0.010 \text{ hr}^{-1}$	$k_c = 1000$	$c_0 = 0.001$	count
Fruit P	$a_P = 0.005 \text{ hr}^{-1}$	$k_P = 0.25$	$P_0 = 0.001$	kg

Table 3: Baseline model parameters for corn. Growth rates are per hour; initial conditions are set to k_x/K where $K \approx 2900$ is the season length in hours.

210 3. Simulation

211 The logistic ODE admits a closed-form solution, enabling exact time-
 212 stepping without numerical integration error. Given state $x(t)$ at time t , the
 213 state at $t + \Delta t$ is:

$$x(t + \Delta t) = \frac{\hat{k}_x(t)}{1 + \left(\frac{\hat{k}_x(t)}{x(t)} - 1 \right) \exp(-\hat{a}_x(t)\Delta t)} \quad (16)$$

214 where $\hat{a}_x(t)$ and $\hat{k}_x(t)$ are treated as constant over the time step. This closed-
 215 form approach is more accurate than forward Euler integration and avoids
 216 instability issues that can arise with explicit methods at larger time steps.

217 We simulate the growing season at hourly resolution ($\Delta t = 1$ hour),
 218 yielding approximately 2900 time steps for a typical corn season (late April
 219 to early October). At each step, we: (1) update the nutrient factors based on
 220 cumulative inputs and divergences, (2) compute effective growth rates and
 221 carrying capacities, and (3) advance each state variable using Equation 16.

222 4. Optimization via genetic algorithm

223 Given the nonlinear, delay-affected dynamics of the crop model, gradient-
 224 based optimization is challenging. The delayed effects of inputs create a
 225 non-convex landscape with potentially many local optima. We therefore
 226 employ a genetic algorithm (GA), a population-based metaheuristic inspired
 227 by natural selection that can effectively explore complex search spaces [14].

228 4.1. Decision variables

229 Each candidate solution encodes a complete irrigation and fertilization
 230 strategy as a four-dimensional vector:

$$\mathbf{u} = \begin{bmatrix} u_1 \\ u_2 \\ u_3 \\ u_4 \end{bmatrix} = \begin{bmatrix} \text{irrigation frequency (hours)} \\ \text{irrigation amount (inches)} \\ \text{fertilizer frequency (hours)} \\ \text{fertilizer amount (lbs)} \end{bmatrix} \quad (17)$$

231 The frequencies specify application intervals: $u_1 = 168$ means irrigate
 232 every 168 hours (weekly). The amounts specify the quantity applied at
 233 each event. This parameterization assumes regular, periodic application—a
 234 simplification that captures common agricultural practice while keeping the
 235 search space tractable.

236 4.2. Objective function

237 The objective is to maximize net revenue, defined as crop value minus
 238 input costs.

$$\text{Revenue}(\mathbf{u}) = \text{Crop Value} - \text{Input Costs} \quad (18)$$

239 The crop value depends on final plant state at harvest:

$$\text{Crop Value} = \omega_h h[K] + \omega_A A[K] + \omega_P P[K] \quad (19)$$

240 where K is the final time step and ω_h , ω_A , ω_P are economic weights (dollars
 241 per unit) for height, leaf area, and fruit biomass respectively.

242 The input costs accumulate over the season:

$$\text{Input Costs} = \omega_w \sum_{k=0}^K w[k] + \omega_f \sum_{k=0}^K f[k] \quad (20)$$

243 where ω_w and ω_f are costs per unit of irrigation and fertilizer.

244 For corn, the economic weights are derived from market prices and typical
 245 yields (Table 4). The fruit biomass weight dominates, reflecting that grain
 246 yield is the primary economic output.

Parameter	Value	Derivation
ω_w	\$2.00/inch	Typical irrigation cost
ω_f	\$0.61/lb	Weighted NPK cost
ω_h	\$35/m	Silage value proxy
ω_A	\$215/m ²	Silage value proxy
ω_P	\$4,450/kg	\$4/bushel \times plant density

Table 4: Economic weights for the corn objective function. The fruit biomass weight accounts for approximately 28,350 plants per acre at \$0.157/kg.

247 *4.3. Algorithm description*

248 The GA maintains a population of M candidate solutions and iteratively
249 improves them through selection, crossover, and mutation over G genera-
250 tions. Algorithm 1 presents the complete procedure.

251 **Selection.** After each generation, population members are ranked by
252 cost. The top P members survive as “parents” for the next generation. This
253 selection ensures the best solutions are never lost.

254 **Crossover.** New “children” are created by blending two parent solutions.
255 For each child, we randomly select two parents and compute a weighted
256 average:

$$\mathbf{u}^{(\text{child})} = \phi \cdot \mathbf{u}^{(a)} + (1 - \phi) \cdot \mathbf{u}^{(b)} \quad (21)$$

257 where $\phi \sim \text{Uniform}(0, 1)$ under normal operation. This crossover can produce
258 children anywhere along the line segment connecting the parents, enabling
259 smooth exploration of the search space.

260 **Mutation and Diversity.** To maintain population diversity and escape
261 local optima, the remaining $M - P - C$ population slots are filled with ran-
262 domly generated solutions. Additionally, if the best cost stagnates (changes
263 by less than 0.01) for 10 consecutive generations, we switch to aggressive
264 crossover with $\phi \sim \text{Uniform}(-1, 2)$. This allows children to lie outside the
265 convex hull of their parents, promoting exploration of new regions.

266 **Default Parameters.** We use $M = 128$ members, $P = 16$ parents,
267 $C = 16$ children, and $G = 100$ generations. The large population relative
268 to generations ensures diversity for exploration while preventing premature
269 convergence.

270 5. Case study: corn in iowa

271 We demonstrate the framework using corn, the most widely planted crop
272 in the United States with over 90 million acres harvested annually [24].
273 The case study uses historical weather data from Fairfax, Iowa (41.76°N ,
274 91.87°W), a representative location in the Corn Belt (USDA climate zones
275 4b–5b).

276 5.1. Scenario configuration

277 The simulation covers a typical growing season from late April to early
278 October (approximately 2900 hours). Environmental inputs are:

- 279 • **Temperature and radiation:** Hourly data from NSRDB for Fairfax,
280 IA. Mean temperature is 22.8°C ; mean solar radiation is 580 W/m^2 .
- 281 • **Precipitation:** Daily data from NOAA, interpolated to hourly reso-
282 lution.
- 283 • **Typical nutrient expectations:** Based on agronomic recommenda-
284 tions [25], the model expects 28 inches of water and 355 lbs of NPK
285 fertilizer over the season ($w_{\text{typ}} \approx 0.01 \text{ in/hr}$, $f_{\text{typ}} \approx 0.12 \text{ lb/hr}$).

286 Table 5 summarizes expected corn development timelines used to calibrate
287 model parameters.

State variable	Days to maturity	Hours to maturity	Typical final value
Plant height h	65–70	1560–1680	2.7–3.7 m
Leaf area A	55–65	1320–1560	0.6–0.7 m^2
Number of leaves N	65	1560	18–20
Spikelets c	65–70	1560–1680	~1000
Fruit biomass P	125	3000	0.15–0.36 kg

Table 5: Corn development timeline and typical final values from agronomic literature [23, 26].

288 5.2. *Baseline scenario: farmer best practices under drought*

289 To establish a performance baseline, we first simulate crop growth under
290 a drought scenario (50% of typical precipitation) using conventional farmer
291 practices: weekly irrigation of 1 inch [27] and monthly fertilizer applications
292 of 90 lbs [28]. These values reflect standard agronomic recommendations for
293 corn in the Corn Belt region.

294 Figure 2 shows the environmental disturbances and control inputs over the
295 growing season. The reduced precipitation characteristic of a drought year is
296 clearly visible, along with the periodic irrigation and fertilizer applications.

297 Figure 3 shows the resulting plant state trajectories. Under drought conditions with conventional management, the plant reaches the following final
298 values: height of 2.6 m (vs. 3.0 m capacity), leaf area of 0.57 m² (vs. 0.65
299 m²), and fruit biomass of 0.22 kg (vs. 0.25 kg). The net revenue under this
300 scenario is \$859/acre.

302 The baseline scenario demonstrates how the model captures stress ef-
303 fects: despite regular irrigation, the mismatch between applied water and
304 the plant's metabolic expectations under drought conditions leads to sus-
305 tained nutrient factor depression and reduced growth potential. Detailed
306 visualizations of the applied vs. absorbed nutrients, cumulative values, and
307 nutrient factors are provided in the Supplementary Information.

308 5.3. Optimization configuration

309 The GA searches over the following bounds:

- 310 • Irrigation frequency: 100–700 hours (4–29 days between applications)
- 311 • Irrigation amount: 0.5–5.0 inches per application
- 312 • Fertilizer frequency: 700–2900 hours (29–121 days, i.e., 1–4 applications per season)
- 314 • Fertilizer amount: 100–500 lbs per application

315 These bounds reflect practical constraints: irrigation systems have minimum application rates, and fertilizer is typically applied in a small number of 316 large doses rather than continuously. The optimization was performed under 317 the same environmental conditions: a drought scenario with 50% of typical 318 precipitation.

320 5.4. Optimization results

321 To assess robustness of the optimization, we executed 10 independent 322 GA runs with different random seeds. Figure 4 shows the convergence of 323 all 10 runs, with each curve representing the best revenue achieved at each 324 generation. All runs converge to similar final values (within 3% of each other), 325 demonstrating that the GA reliably finds near-optimal solutions despite the 326 stochastic nature of the search.

327 The optimal strategy identified by the GA is summarized in Table 6. 328 Notably, the algorithm discovers a strategy with less frequent but larger 329 irrigation events and infrequent fertilizer applications—a pattern that mini- 330 mizes cumulative divergence from expected nutrient levels given the model’s 331 delayed absorption dynamics.

Parameter	Optimal Value	Interpretation
Irrigation frequency	1237 hours	Every \sim 7 weeks
Irrigation amount	5 inches	Per application
Fertilizer frequency	803 hours	Every 33 days
Fertilizer amount	77 lbs	Per application

Table 6: Optimal irrigation and fertilization strategy identified by the GA.

332 Figure 5 shows the plant state trajectories for the best member in each of
333 the 10 GA runs. All optimized strategies achieve substantially higher final
334 values than the baseline farmer practices: fruit biomass ranges from 0.168–
335 0.225 kg (vs. 0.22 kg baseline), heights reach 2.41–2.88 m (vs. 2.6 m), leaf
336 areas reach 0.44–0.56 m² (vs. 0.57 m²), and revenues reach 778–999 \$/acre
337 (vs. \$859/acre baseline). The consistency across runs further confirms the
338 robustness of the optimization, and while the farmer best practice yields
339 higher revenue than one GA run (run 2), in aggregate, the GA optimization
340 meaningfully improved upon the baseline.

341 Table 7 provides an economic comparison between the baseline farmer
 342 practices and the GA-optimized strategies. The best GA strategy achieves
 343 \$999/acre net revenue compared to \$859/acre for the baseline—a 16% im-
 344 provement. Even the worst members in each GA run’s final population out-
 345 perform the baseline, providing a sanity check that random strategies are not
 346 viable (see Supplementary Information).

Metric	GA-Optimized	Baseline
Final fruit biomass	0.22 kg	0.22 kg
Final height	2.8 m	2.6 m
Final leaf area	0.60 m ²	0.57 m ²
Total irrigation	15 inches	18 inches
Total fertilizer	307 lbs	450 lbs
Crop value	\$1218	\$1171
Input costs	\$219	\$312
Revenue	\$999	\$859

Table 7: Economic comparison of GA-optimized versus baseline farmer strategies. The optimized strategy achieves 16% higher net revenue through both increased crop value and dramatically reduced irrigation costs.

347 6. Discussion

348 6.1. Interpretation of results

349 The GA-optimized strategy differs from conventional wisdom in several
 350 notable ways. The algorithm discovers that less frequent but larger irrigation
 351 events, combined with reduced total fertilizer input, can outperform conven-
 352 tional uniform application schedules. This counterintuitive result emerges
 353 from the model’s delayed absorption dynamics: under drought conditions,
 354 the plant’s metabolic expectations are calibrated to typical water availabil-
 355 ity. The GA discovers that strategically-timed resource inputs better main-
 356 tain alignment with metabolic expectations than aggressive compensation
 357 for drought through frequent, uniform applications.

358 The consistency across 10 independent GA runs provides confidence that
 359 the optimization reliably identifies high-performing regions of the strategy
 360 space. While individual runs converge to somewhat different local optima
 361 (with revenues ranging from \$778 to \$983 per acre), 9 of 10 runs outperform

362 the baseline farmer practices, demonstrating the robustness of the optimization
363 approach. The sanity check showing that even the worst members in
364 each final population generally outperform baseline practices confirms that
365 the GA successfully eliminates poor candidates.

366 The 16% revenue improvement (\$999 vs. \$859 per acre) demonstrates sub-
367 substantial potential value from model-based optimization. This improvement
368 comes from two sources: (1) increased crop value due to better-aligned nu-
369 trient delivery, and (2) reduced input costs. The result suggests that conven-
370 tional wisdom about drought response—applying more water to compensate—
371 may be suboptimal when plant physiology involves delayed, cumulative-effect
372 dynamics.

373 6.2. Parameter estimation in practice

374 The framework requires crop-specific parameters: growth rates, carrying
375 capacities, metabolic timescales, and typical nutrient expectations. Several
376 approaches could estimate these from data:

- 377 • **Growth curves:** Time-series imagery from field cameras or drones,
378 processed with computer vision, could provide height and leaf area
379 trajectories for fitting a_x and k_x parameters.
- 380 • **Metabolic timescales:** The temporal spreads σ could be estimated
381 from controlled experiments varying input timing, or inferred from
382 physiological literature on nutrient uptake rates.
- 383 • **Typical expectations:** Regional agronomic recommendations pro-
384 vide baseline values for w_{typ} , f_{typ} , T_{typ} , and R_{typ} .

385 Physics-informed neural networks (PINNs) could jointly fit model param-
386 eters and approximate unknown functional forms in the dynamics, potentially
387 relaxing some of the structural assumptions in Section 2.

388 6.3. Limitations and extensions

389 Several model limitations suggest directions for future work:

390 **Growth model.** The logistic equation assumes symmetric growth around
391 the inflection point. Richards growth [29] generalizes this with a shape pa-
392 rameter ν :

$$\frac{dx}{dt} = a_x x \left[1 - \left(\frac{x}{k_x} \right)^\nu \right] \quad (22)$$

393 where $\nu > 1$ produces steeper early growth (common in vegetative stages)
394 and $\nu < 1$ produces steeper late growth.

395 **Absorption kernels.** Gaussian kernels are symmetric, but physiological
396 absorption often exhibits fast activation followed by slow decay. Log-normal
397 or Gamma kernels could better capture this asymmetry.

398 **Saturation.** The current model does not explicitly limit nutrient uptake—
399 all applied inputs eventually affect the plant. In reality, excess application
400 may be lost to runoff or leaching. Saturating nonlinearities in the absorption
401 pathway would provide a more realistic response to over-application.

402 **Spatial heterogeneity.** The model treats a single representative plant.
403 Field-scale optimization would need to account for spatial variation in soil
404 properties, microclimate, and plant density.

405 **Stochastic weather.** The case study uses historical weather data. Ro-
406 bust optimization under weather uncertainty, or adaptive strategies that re-
407 spond to observed conditions, could improve real-world performance.

408 7. Conclusion

409 This paper presented a coupled ODE model for crop growth that cap-
410 tures delayed nutrient absorption via FIR convolution and cumulative stress
411 effects via EMA filtering. The model’s time-varying growth rates and carry-
412 ing capacities encode the intuition that plant development depends not just
413 on current conditions but on the history of resource availability relative to
414 physiological expectations.

415 Applied to corn optimization in Iowa under drought conditions, a ge-
416 netic algorithm discovered irrigation and fertilizer strategies that achieve
417 16% higher net revenue than conventional farmer practices (\$999 vs. \$859
418 per acre). This improvement emerges from the model’s delayed absorption
419 dynamics: strategic timing of inputs that aligns with metabolic expectations
420 outperforms uniform application schedules. The consistency across 10 inde-
421 pendent optimization runs, with 9 of 10 outperforming the baseline, confirms
422 the robustness of these findings.

423 The framework is generalizable to other crops through re-parameterization
424 and offers a computationally tractable approach to input optimization. Fu-
425 ture work will extend the model to handle weather uncertainty, incorporate
426 spatial heterogeneity, and validate predictions against field trial data.

⁴²⁷ **8. Supplementary information**

⁴²⁸ This supplementary section provides additional visualizations of the base-
⁴²⁹ line scenario (farmer best practices under drought) and the GA optimization
⁴³⁰ results.

⁴³¹ *S1. Detailed baseline scenario analysis*

⁴³² Figure 6 shows the applied versus absorbed nutrients under the baseline
⁴³³ scenario. The delayed absorption via FIR convolution is clearly visible: the
⁴³⁴ absorbed signals (smoothed curves) lag behind the applied inputs and exhibit
⁴³⁵ the characteristic spreading effect of the Gaussian kernels.

⁴³⁶ Figure 7 shows the cumulative absorbed nutrients compared to expected
⁴³⁷ (typical) levels. Under drought conditions, actual water absorption falls pro-
⁴³⁸ gressively below expectations, while fertilizer, temperature, and radiation
⁴³⁹ track more closely to typical values.

⁴⁴⁰ Figure 8 shows the instantaneous divergence from expected cumulative
⁴⁴¹ levels. These divergences, after EMA smoothing, determine the nutrient
⁴⁴² factors that modulate plant growth.

⁴⁴³ Figure 9 shows the resulting nutrient factors. The water factor ν_w declines
⁴⁴⁴ throughout the season as drought stress accumulates, reaching approximately
⁴⁴⁵ 0.6 by harvest. This reduced water factor is the primary driver of the sub-
⁴⁴⁶ optimal crop growth observed in the baseline scenario.

447 *S2. GA optimization: worst-case analysis*

448 As a sanity check, Figure 10 shows the plant state trajectories for the
449 *worst* member in each GA run’s final population. Even these subopti-
450 mal strategies—the least fit survivors after 100 generations of evolution—
451 outperform the baseline farmer practices. This confirms that: (1) the GA
452 successfully eliminates poor strategies, and (2) random or arbitrary irri-
453 gation/fertilization schedules cannot match even the worst optimized ap-
454 proaches.

455 **9. Acknowledgements**

456 This work has been partially supported by the UC Berkeley College of
457 Engineering and the USDA AI Institute for Next Generation Food Systems
458 (AIFS), USDA award number 2020-67021-32855.

459 **Declarations**

460 **Competing Interests** The authors declare that they have no known com-
461 peting financial interests or personal relationships that could have appeared
462 to influence the work reported in this paper.

463 **Code availability** The source code used for this study is archived on Zen-
464 odo at <https://doi.org/10.5281/zenodo.18204023>.

466 **Declaration of generative AI and AI-assisted technologies in the
467 manuscript preparation process** During the preparation of this work the
468 authors used ChatGPT and Claude Code in order to generate some portions
469 of the code base, though no underlying theory, and refine the original drafts of
470 the paper. After using this tool/service, the authors reviewed and edited the
471 content as needed and take full responsibility for the content of the published
472 article.

474 **References**

- 475 [1] Economic Research Service, Farm income and wealth statistics, US
476 Department of Agriculture (2024).
477 URL [https://www.ers.usda.gov/data-products/
478 farm-income-and-wealth-statistics/](https://www.ers.usda.gov/data-products/farm-income-and-wealth-statistics/)
- 479 [2] T. I. Zohdi, A machine-learning enabled digital-twin framework for
480 next generation precision agriculture and forestry, Computer Meth-
481 ods in Applied Mechanics and Engineering 428 (2024) 117250. doi:
482 [10.1016/j.cma.2024.117250](https://doi.org/10.1016/j.cma.2024.117250).
- 483 [3] E. Mengi, C. J. Becker, M. Sedky, S. Yu, T. I. Zohdi, A digital-twin
484 and rapid optimization framework for optical design of indoor farming
485 systems, Computational Mechanics 72 (2023) 953–970. doi:[10.1007/s00466-023-02421-9](https://doi.org/10.1007/s00466-023-02421-9).

- 487 [4] P. Goodrich, O. Betancourt, A. Arias, T. I. Zohdi, Placement and drone
488 flight path mapping of agricultural soil sensors using machine learning,
489 Computers and Electronics in Agriculture 198 (2022) 107591. doi:10.
490 1016/j.compag.2022.107591.
- 491 [5] I. Tagkopoulos, S. F. Brown, X. Liu, Q. Zhao, T. I. Zohdi, J. M. Earles,
492 N. Nitin, D. E. Runcie, D. G. Lemay, A. D. Smith, P. C. Ronald, H. Feng,
493 G. D. Youtsey, Special report: AI institute for next generation food
494 systems (AIFS), Computers and Electronics in Agriculture 196 (2022)
495 106819. doi:10.1016/j.compag.2022.106819.
- 496 [6] P.-F. Verhulst, Notice sur la loi que la population suit dans son accroissement,
497 Correspondance mathématique et physique 10 (1838) 113–126.
498 doi:10.1007/BF02309004.
- 499 [7] J. W. Jones, G. Hoogenboom, C. H. Porter, K. J. Boote, W. D. Batchelor,
500 L. Hunt, P. W. Wilkens, U. Singh, A. J. Gijsman, J. T. Ritchie, The
501 dssat cropping system model, European Journal of Agronomy 18 (3-4)
502 (2003) 235–265. doi:10.1016/S1161-0301(02)00107-7.
- 503 [8] D. P. Holzworth, N. I. Huth, P. G. deVoil, E. J. Zurcher, N. I. Herrmann,
504 G. McLean, K. Chenu, E. J. van Oosterom, V. Snow, C. Murphy,
505 et al., Apsim—evolution towards a new generation of agricultural systems
506 simulation, Environmental Modelling & Software 62 (2014) 327–350.
507 doi:10.1016/j.envsoft.2014.07.009.
- 508 [9] C. Van Diepen, J. Wolf, H. Van Keulen, C. Rappoldt, Wofost: a simu-
509 lation model of crop production, Soil Use and Management 5 (1) (1989)
510 16–24. doi:10.1111/j.1475-2743.1989.tb00755.x.
- 511 [10] R. Gebbers, V. I. Adamchuk, Precision agriculture and food security,
512 Science 327 (5967) (2010) 828–831. doi:10.1126/science.1183899.
- 513 [11] A. Singh, An overview of the optimization modelling applications, Jour-
514 nal of Hydrology 466–467 (2012) 167–182. doi:10.1016/j.jhydrol.
515 2012.08.004.
- 516 [12] J. E. Epperson, J. E. Hook, Y. R. Mustafa, Dynamic program-
517 ming for improving irrigation scheduling strategies of maize,
518 Agricultural Systems 42 (1) (1993) 85–101, applications of

- 519 Dynamic Optimization Techniques to Agricultural Problems.
520 doi:[https://doi.org/10.1016/0308-521X\(93\)90070-I](https://doi.org/10.1016/0308-521X(93)90070-I).
521 URL <https://www.sciencedirect.com/science/article/pii/0308521X9390070I>
- 523 [13] W. Ding, C. Lin, Application of genetic algorithms to agriculture: a
524 review, Computers and Electronics in Agriculture 175 (2020) 105524.
525 doi:[10.1016/j.compag.2020.105524](https://doi.org/10.1016/j.compag.2020.105524).
- 526 [14] D. E. Goldberg, Genetic Algorithms in Search, Optimization, and Ma-
527 chine Learning, Addison-Wesley, Reading, MA, 1989.
- 528 [15] R. Wardlaw, K. Bhaktikul, Application of genetic algorithms for irriga-
529 tion water scheduling, Irrigation and Drainage 53 (4) (2004) 397–414.
530 doi:[10.1002/ird.121](https://doi.org/10.1002/ird.121).
- 531 [16] Z. Yu, W. Fu, Optimization of nitrogen fertilization strategies for drip
532 irrigation of cotton in large fields by dssat combined with a genetic
533 algorithm, Applied Sciences 15 (7) (2025) 3580.
- 534 [17] M. Sengupta, Y. Xie, A. Lopez, A. Habte, G. MacLaurin, J. Shelby, The
535 national solar radiation data base (nsrdb), Renewable and Sustainable
536 Energy Reviews 89 (2018) 51–60. doi:[10.1016/j.rser.2018.03.003](https://doi.org/10.1016/j.rser.2018.03.003).
- 537 [18] National Oceanic and Atmospheric Administration, Climate data online
538 (2024).
539 URL <https://www.ncdc.noaa.gov/cdo-web/>
- 540 [19] J. E. Sawyer, E. D. Nafziger, G. W. Randall, L. G. Bundy, G. W.
541 Rehm, B. C. Joern, Nitrogen management for corn production, Iowa
542 State University Extension Publication PM 1714 (2006).
- 543 [20] J. O. Payero, D. D. Tarkalson, S. Irmak, D. R. Davison, J. L. Petersen,
544 Effect of irrigation amounts applied with subsurface drip irrigation on
545 corn evapotranspiration, yield, water use efficiency, and dry matter pro-
546 duction in a semiarid climate, Agricultural Water Management 95 (8)
547 (2008) 895–908. doi:[10.1016/j.agwat.2008.02.015](https://doi.org/10.1016/j.agwat.2008.02.015).
- 548 [21] B. Sánchez, A. Rasmussen, J. R. Porter, Temperatures and the growth
549 and development of maize and rice: a review, Global Change Biology
550 20 (2) (2014) 408–417. doi:[10.1111/gcb.12389](https://doi.org/10.1111/gcb.12389).

- 551 [22] R. C. Lewontin, D. Cohen, On population growth in a randomly varying
552 environment, *Proceedings of the National Academy of Sciences* 62 (4)
553 (1969) 1056–1060. doi:10.1073/pnas.62.4.1056.
- 554 [23] L. J. Abendroth, R. W. Elmore, M. J. Boyer, S. K. Marlay, In corn
555 growth and development, Iowa State University Extension Publication
556 PMR 1009 (2011).
- 557 [24] US Department of Agriculture, 2023 acreage data as of august 9, 2023
558 (2023).
- 559 [25] J. Sawyer, E. Nafziger, G. Randall, L. Bundy, G. Rehm, B. Joern, Con-
560 cepts and rational for regional nitrogen rate guidelines for corn, Univer-
561 sity Extension Iowa State University Ames (2006).
- 562 [26] F. Schierbaum, Book reviews: Corn: Chemistry and technology, 2nd
563 edition. by pamela j. white and lawrence a. johnson (editors), Starch-
564 starke - STARCH 56 (2004) 263–264. doi:10.1002/star.200490027.
- 565 [27] W. L. Kranz, S. Irmak, S. J. van Donk, C. D. Yonts, D. L. Martin, Irri-
566 gation management for corn, Tech. Rep. G1850, University of Nebraska–
567 Lincoln Extension (2008).
568 URL <https://extensionpubs.unl.edu/publication/g1850/>
- 569 [28] B. Davies, J. A. Coulter, P. H. Pagliari, Timing and rate of nitrogen
570 fertilization influence maize yield and nitrogen use efficiency, *PLOS ONE*
571 15 (5) (2020) e0233674. doi:10.1371/journal.pone.0233674.
- 572 [29] F. J. Richards, A flexible growth function for empirical use, *Journal of*
573 *Experimental Botany* 10 (2) (1959) 290–301. doi:10.1093/jxb/10.2.
574 290.

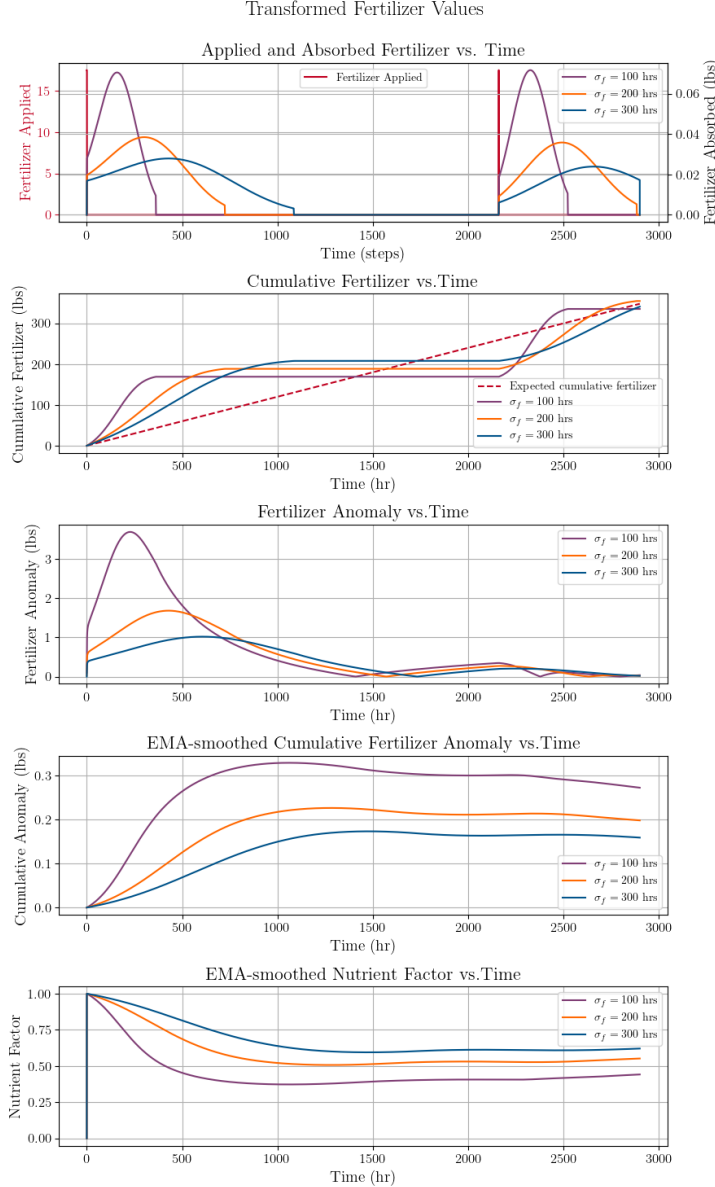


Figure 1: Illustration of the metabolic transformation pipeline. Panel 1: Gaussian FIR kernels with different temporal spreads σ demonstrate how water ($\sigma_w = 30$ hr) is absorbed more rapidly than fertilizer ($\sigma_f = 300$ hr). Panel 4: EMA filters with different memory parameters β show how cumulative divergence tracking responds to sustained anomalies, with larger β providing longer memory of past stress events.

Algorithm 1 Genetic Algorithm for Input Optimization

- 1: **Input:** Population size M , parents P , children C , generations G , bounds $[\mathbf{u}_{\min}, \mathbf{u}_{\max}]$
- 2: **Output:** Best solution \mathbf{u}^*
- 3:
- 4: Initialize population $\{\mathbf{u}^{(1)}, \dots, \mathbf{u}^{(M)}\}$ uniformly in bounds
- 5: Evaluate Cost($\mathbf{u}^{(i)}$) for all i via full-season simulation
- 6: Sort population by cost (ascending)
- 7: stagnation $\leftarrow 0$
- 8:
- 9: **for** $g = 1$ to G **do**
- 10: **Selection:** Keep top P members as parents
- 11:
- 12: **Crossover:** Generate C children
- 13: **for** $j = 1$ to C **do**
- 14: Select parents $\mathbf{u}^{(a)}, \mathbf{u}^{(b)}$ randomly from top P
- 15: **if** stagnation < 10 **then**
- 16: $\phi \sim \text{Uniform}(0, 1)$
- 17: **else**
- 18: $\phi \sim \text{Uniform}(-1, 2)$ ▷ Aggressive exploration
- 19: **end if**
- 20: $\mathbf{u}^{(\text{child})} \leftarrow \phi \cdot \mathbf{u}^{(a)} + (1 - \phi) \cdot \mathbf{u}^{(b)}$
- 21: Clip to bounds
- 22: **end for**
- 23:
- 24: **Fill remaining:** Generate $M - P - C$ random members
- 25: Evaluate costs for new members
- 26: Sort population by cost
- 27:
- 28: **Stagnation check:**
- 29: **if** $|\text{Cost}^{(g)} - \text{Cost}^{(g-1)}| < 0.01$ **then**
- 30: stagnation \leftarrow stagnation + 1
- 31: **else**
- 32: stagnation $\leftarrow 0$
- 33: **end if**
- 34: **end for**
- 35:
- 36: **return** $\mathbf{u}^{(1)}$ (best member)

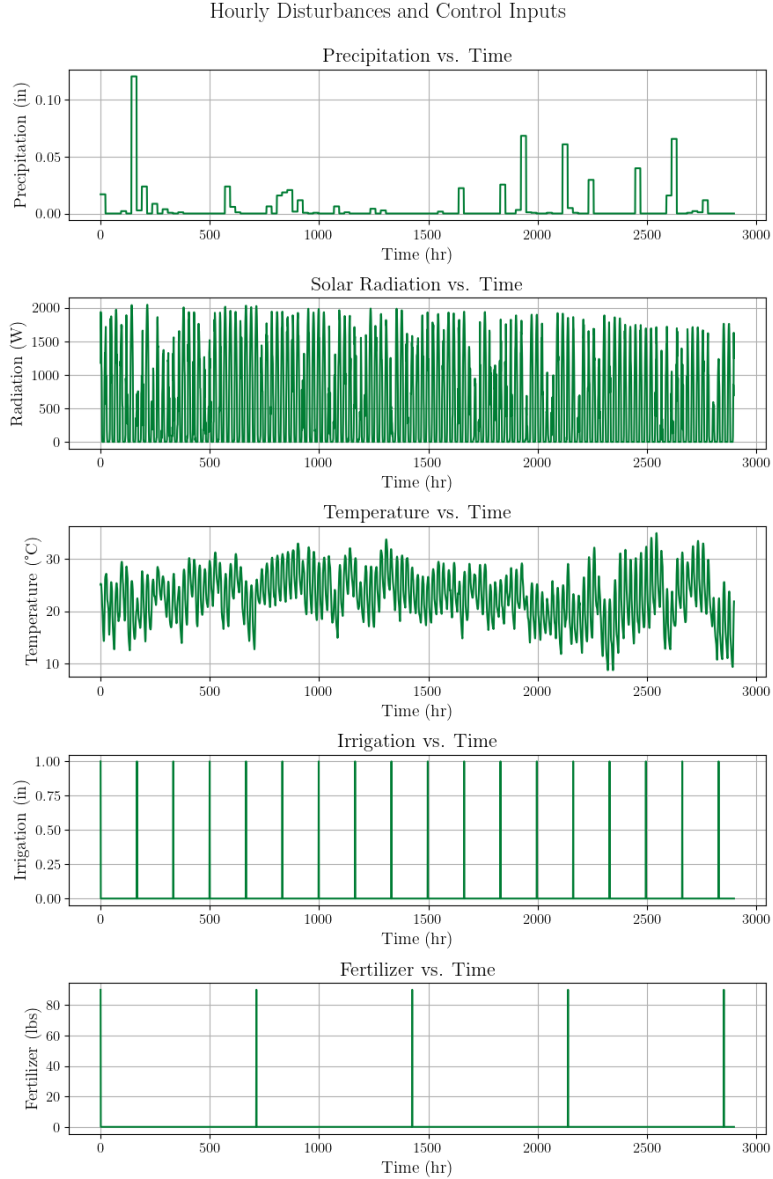


Figure 2: Environmental disturbances and control inputs for the baseline scenario. Top three panels show hourly precipitation (reduced to 50% of normal), solar radiation, and temperature from historical Iowa data. Bottom two panels show the farmer's irrigation (weekly, 1 inch) and fertilizer (monthly, 90 lbs) application strategy.

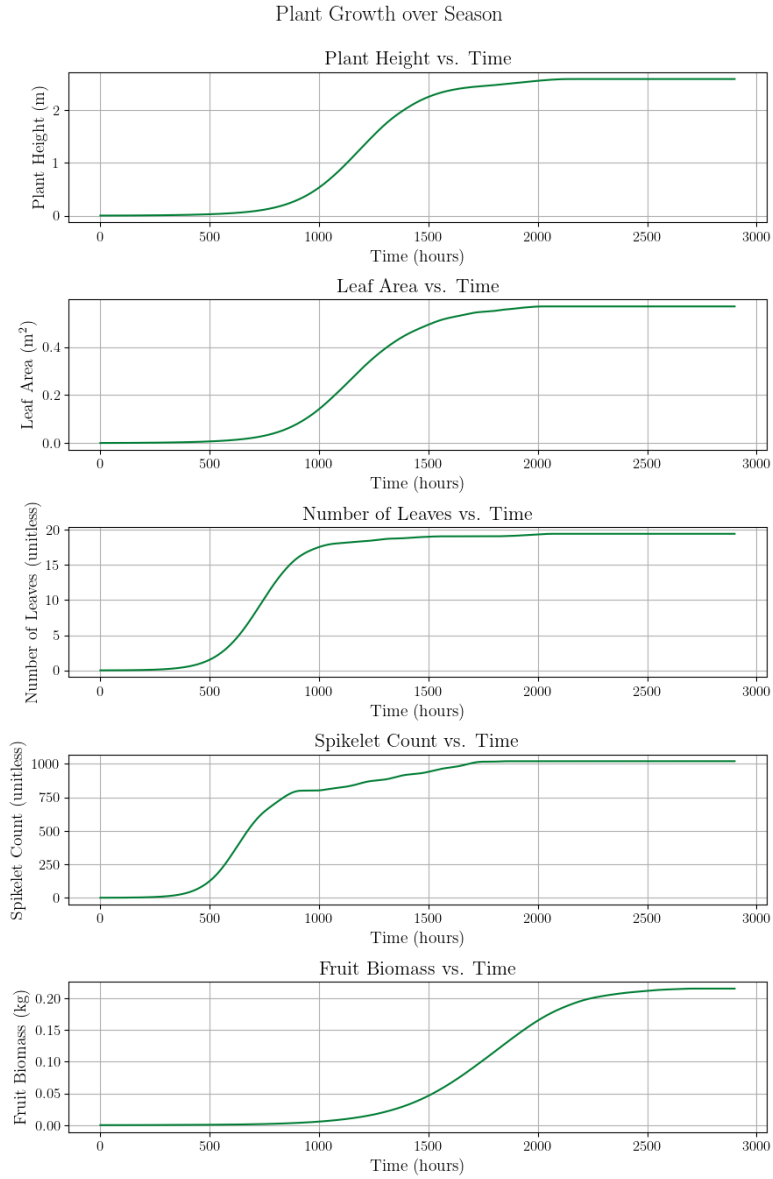


Figure 3: Plant state variable trajectories under the baseline scenario (farmer best practices during drought). All state variables reach suboptimal final values due to cumulative water stress. This strategy yields \$859/acre in revenue.

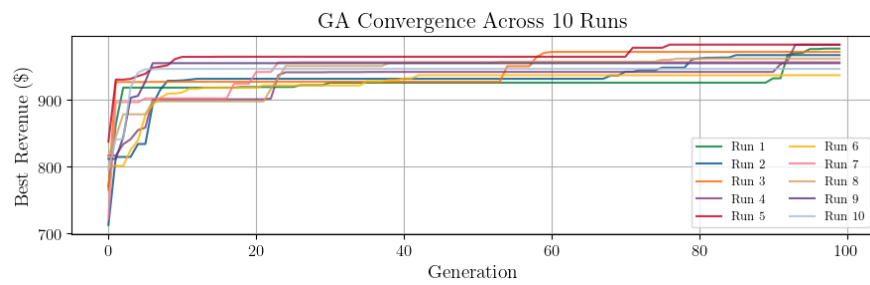


Figure 4: GA convergence across 10 independent runs. Each curve shows the best revenue at each generation. All runs exhibit rapid improvement in early generations followed by convergence to near-optimal solutions. The consistency across runs demonstrates algorithm robustness.

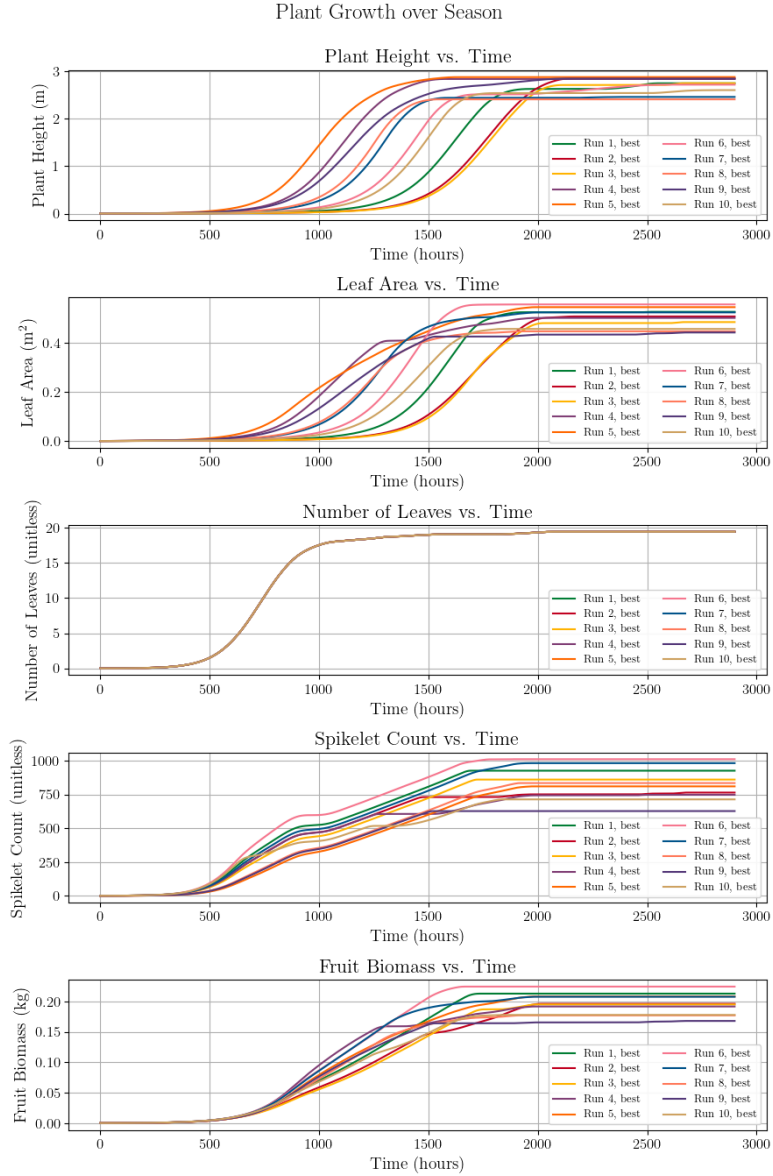


Figure 5: Plant state variable trajectories for the best member from each of the 10 independent GA runs. All optimized strategies achieve similar, near-optimal growth trajectories, and 9 of 10 runs substantially outperform the baseline farmer practices (Figure 3). The tight clustering of trajectories demonstrates that different GA runs converge to similar optimal strategies.

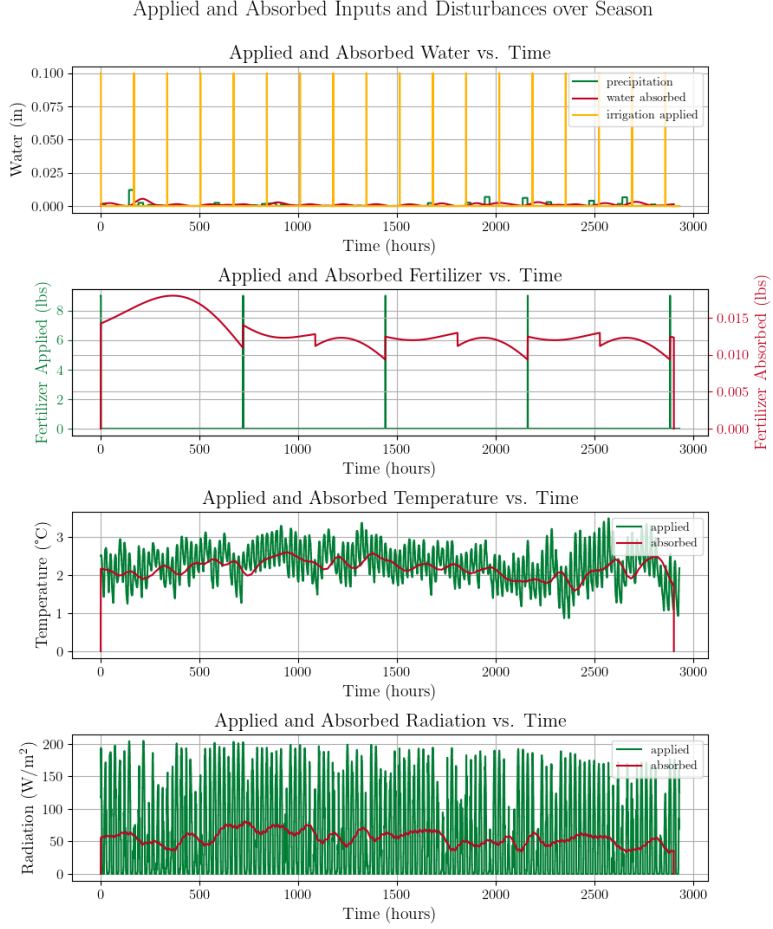


Figure 6: Applied versus absorbed nutrients under the baseline farmer strategy. The delayed absorption dynamics are evident in the lag between applied inputs and the smoothed absorbed signals. Water absorption ($\sigma_w = 30$ hr) responds more quickly than fertilizer absorption ($\sigma_f = 300$ hr).

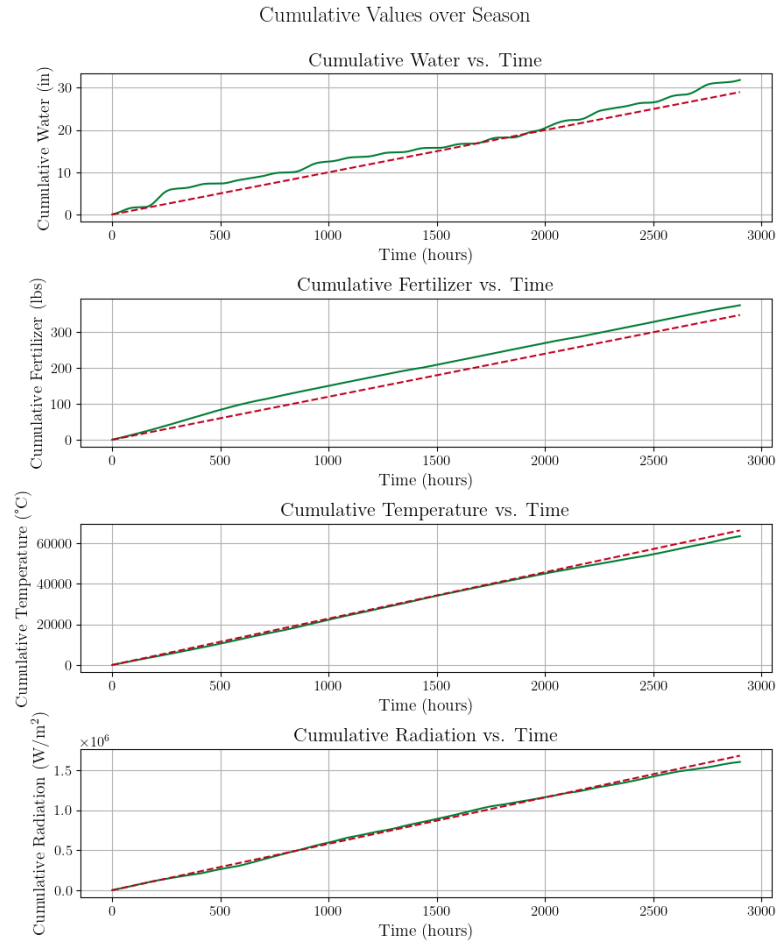


Figure 7: Cumulative absorbed nutrients (solid) versus expected levels (dashed red). The growing gap between actual and expected water absorption reflects the drought stress accumulating over the season. Fertilizer applications maintain closer alignment with expectations.

Differences between Actual and Typical Cumulative Values

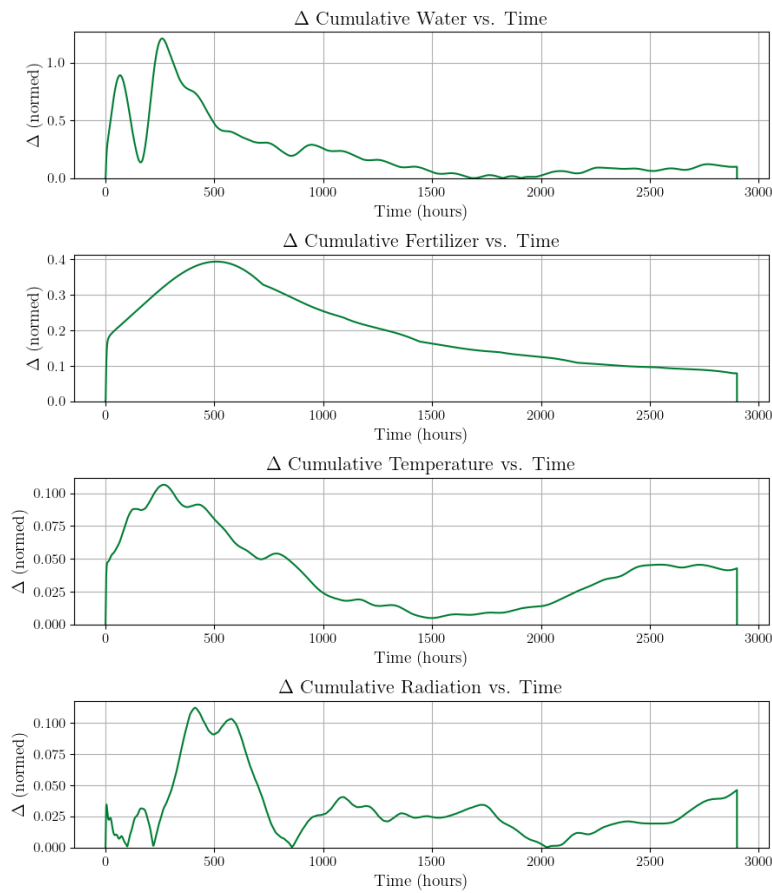


Figure 8: Instantaneous divergence from expected cumulative nutrient levels. Higher divergence indicates greater stress. The water divergence grows throughout the season due to cumulative drought effects.

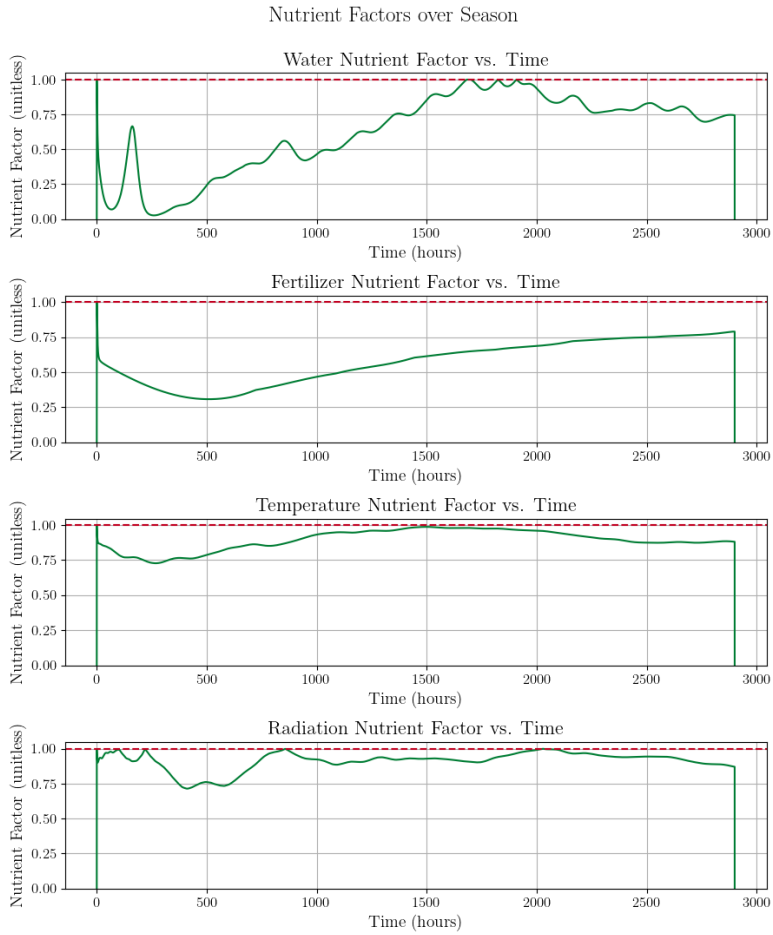


Figure 9: Nutrient factor evolution under the baseline scenario. The water factor ν_w declines due to cumulative drought stress, while fertilizer, temperature, and radiation factors remain closer to 1.0 (no stress). The declining ν_w reduces effective growth rates and carrying capacities throughout the season.

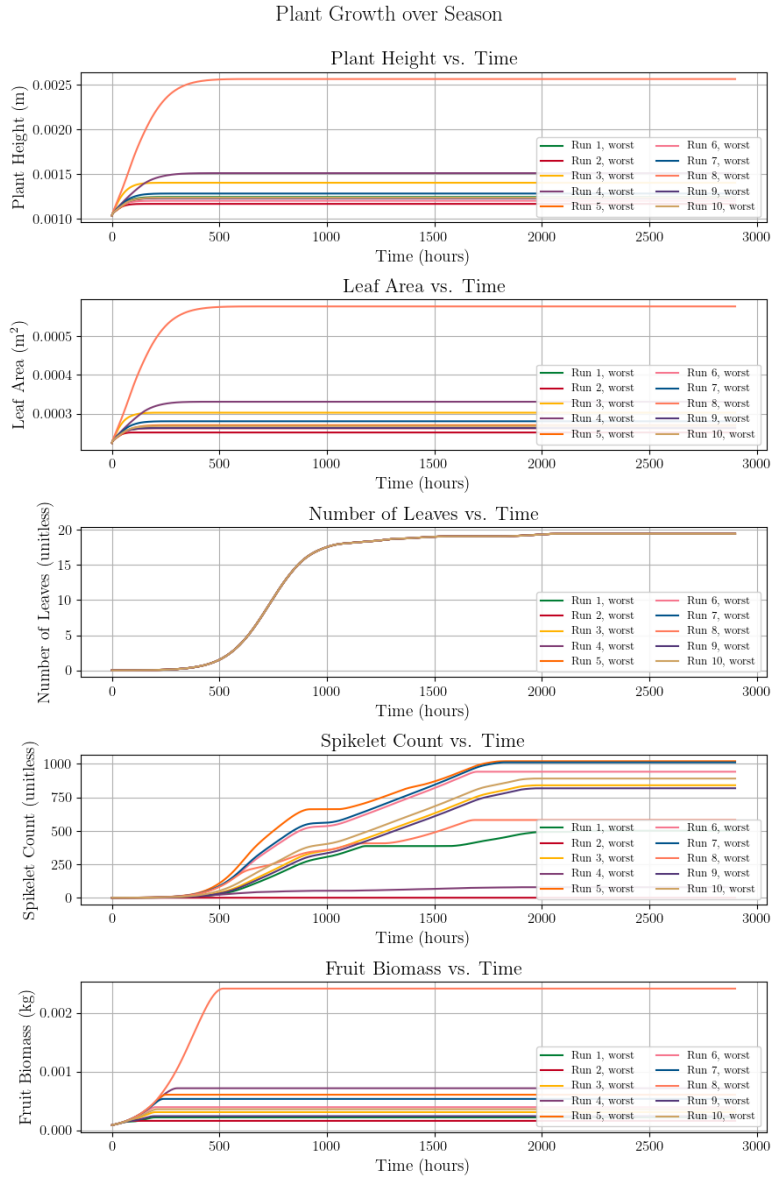


Figure 10: Plant state variable trajectories for the worst member from each GA run's final population. Even these suboptimal strategies outperform baseline farmer practices (compare to Figure 3), demonstrating that the GA successfully identifies the high-performing region of the strategy space and that random strategies are not competitive.